[MS. Ref. No.: MICMAT-D-12-01120]

Microporous cesium salts of tetravalent Keggin-type polyoxotungstates $Cs_4[SiW_{12}O_{40}]$, $Cs_4[PW_{11}O_{39}(Sn\text{-}n\text{-}C_4H_9)]$, and $Cs_4[PW_{11}O_{39}(Sn\text{-}OH)]$ and their adsorption properties

Yu-ki Miura[a], Hiroyuki Imai[b], Toshiyuki Yokoi[c], Takashi Tatsumi[c], Yuichi Kamiya[d,*]

[a]Graduate School of Environmental Science, Hokkaido University, Nishi 5, Kita 10, Kita-ku, Sapporo 060-0810, Japan

[b]Department of Chemical Engineering, The University of Kitakyushu, 1-1, Hibikino, Wakamatsu-ku, Kitakyushu, Fukuoka, 808-0135, Japan

[c]Chemical Research Laboratory, Tokyo Institute of Technology, Nagatsuta 4259, Midori-ku, Yokohama 226-8503, Japan

[d]Research Faculty of Environmental Earth Science, Hokkaido University, Nishi 5, Kita 10, Kita-ku, Sapporo 060-0810, Japan

*Corresponding author. Tel./fax: +81-11-706-2217. *E-mail address*: kamiya@ees.hokudai.ac.jp

ABSTRACT

Microporous cesium salts of modified and unmodified tetravalent Keggin-type polyoxometalates, including $Cs_4[SiW_{12}O_{40}]$, $Cs_4[PW_{11}O_{39}(Sn\text{-}n\text{-}C_4H_9)]$, and $Cs_4[PW_{11}O_{39}(Sn\text{-}OH)]$, were synthesized. The crystalline structures, which had body-centered cubic (bcc) arrangements, the lattice constants, and the pore-size distributions of the three Cs salts were similar, regardless of the presence or absence and types of functional groups introduced. The Cs salts had only micropores and no mesopores. The micropore size distributions were determined from adsorption isotherms of Ar, which showed a sharp peak at 0.59 nm and a shoulder at 0.62 nm. The fractions of the external surface areas to the total surface areas of the Cs salts were less than 6%. It is plausible that the micropores originate from the heteropoly anion defects in the crystallite, which form to avoid mismatches in the Cs^+/(heteropoly anion) ratio required for charge balance (= 4) and for a bcc structure (= 3). The surface of the Cs salt introduced with *n*-butyl groups was hydrophobic, although the surface density of the *n*-butyl groups was low. On the other hand, the hydroxyl groups present on the surface of $Cs_4[PW_{11}O_{39}(Sn\text{-}OH)]$ had little effect on the adsorption of water, methanol, ethanol, and hexane but a great impact on that for benzene due to the interactions between the -OH groups and the aromatic rings (-OH$\cdots\pi$).

Keywords: Heteropoly acid; Hydrophobicity; Microporous material; Adsorption property; Anion defect

1. Introduction

Ionic crystals, which are important families of crystalline materials, have been attracting considerable interest because of their unique chemical and physical properties, which depend on their crystalline structures and constituent ions [1–9]. Normally, cations and anions are densely packed in the crystal lattice, with the coordination numbers determined by the relative sizes and charges of the constituent ions since the Coulombic forces are strong and directionless. Therefore, most ionic crystals do not have structural micropores caused by the crystal structure, unlike crystalline aluminosilicates, and thus, they only have low surface areas. However, by using the proper sizes, charges, and compositions of the constituent ions as well as precise control of the preparation conditions, some ionic crystals become porous [10,11].

An example of porous ionic crystals is a series of polyoxometalate salts with macrocations [2,6,12–15]. Polyoxometalates with a Keggin structure ($[XW_{12}O_{40}]^{n-}$, abbreviated as *Keggin-POM*) are nano-sized metal-oxide multivalent anions with well-defined molecular structures. Although the salts of *Keggin-POMs* normally do not have intrinsic micropores in the crystal lattice, like conventional ionic crystals, *Keggin-POM* salts with macrocations, such as oxo-bridged trinuclear chromium carboxylate ($[Cr_3O(OOCR)]^+$), have intrinsic pores in the crystal lattice and show unique adsorption properties, which depend on the types of organic groups on the

macrocation and the residual counter cations [16–18].

On the other hand, in some cases, *Keggin-POM* salts form microporous solids even when relatively small cations, like Cs^+ and NH_4^+, are used as counter cations [19–25]. Among them, the crystal and pore structures of acidic and neutral Cs salts of a trivalent *Keggin-POM* ($Cs_xH_{3-x}[PW_{12}O_{40}]$) have been extensively studied [26–28]. The pore structures of $Cs_xH_{3-x}[PW_{12}O_{40}]$ are very sensitive to the Cs^+ ion content [29]. It has been reported that $Cs_{2.1}H_{0.9}[PW_{12}O_{40}]$ is microporous. This *Keggin-POM* salt acts as a size-selective catalyst for acid-catalyzed reactions [30], whereas the pores of $Cs_xH_{3-x}[PW_{12}O_{40}]$ with $x \geq 2.3$ show bimodal distributions, ranging from microporous to mesoporous [29].

In contrast to $Cs_xH_{3-x}[PW_{12}O_{40}]$, there are only a few reports involving Cs salts of tetravalent *Keggin-POMs* like $[SiW_{12}O_{40}]^{4-}$, although the molecular structure of $[SiW_{12}O_{40}]^{4-}$ is similar to that of $[PW_{12}O_{40}]^{3-}$. The major difference between $[PW_{12}O_{40}]^{3-}$ and $[SiW_{12}O_{40}]^{4-}$ is the electronic charges, which are –3 and –4, respectively. Moffat et al. have reported that the neutral Cs salt $Cs_4[SiW_{12}O_{40}]$ has micropores and a high surface area (150 $m^2\ g^{-1}$) [31]. However, the size of the micropores is uncertain. Pizzio and Blanco have reported the synthesis of acidic Cs salts, $Cs_{3.4}H_{0.6}[SiW_{12}O_{40}]$ and $Cs_{3.8}H_{0.2}[SiW_{12}O_{40}]$, and that they act as acid catalysts towards phenol tetrahydropyranylation [32]. However, these microporous Cs salts also have well-developed

mesopores.

The hydrophobicity of the solid surface is a critical factor affecting the adsorption properties of solid materials. Modification of the surface with alkyl groups and fluorine enhances the hydrophobicity, leading to unique adsorption properties [33–36]. Kuwahara et al. have demonstrated that the hydrophobicities of Y-type zeolites significantly increase upon modification with triethoxyfluorosilane [37]. Inumaru et al. have reported that mesoporous silica MCM-41, whose mesopore walls were grafted with *n*-octyl groups, selectively incorporates 4-nonlylphenol and 4-*n*-heptylaniline into its mesopores from aqueous phases due to strong interactions between the hydrophobic surface and the substrates [38].

In our previous communication [39], we have reported that microporous $Cs_xH_{4-x}[SiW_{12}O_{40}]$ with highly developed micropores forms when $x > 2$ and the titration speed of an aqueous Cs_2CO_3 solution to an aqueous $H_4SiW_{12}O_{40}$ solution is carefully controlled. In addition, the acidic Cs salt $Cs_3H[SiW_{12}O_{40}]$ acts as a size-selective catalyst towards acid-catalyzed reactions in the liquid phase due to its uniform micropores and small external surface area.

Here we expand on our previous findings that Cs salts of the tetravalent *Keggin-POM* $[SiW_{12}O_{40}]^{4-}$ formed microporous ionic crystals with the Cs salts of other tetravalent *Keggin-POMs* modified with *n*-butyl and hydroxyl groups, $[PW_{11}O_{39}(Sn\text{-}n\text{-}C_4H_9)]^{4-}$ and $[PW_{11}O_{39}(Sn\text{-}OH)]^{4-}$ (Fig.

1). In the present study, we investigated the molecular and crystalline structures of the neutral Cs salts of $[SiW_{12}O_{40}]^{4-}$, $[PW_{11}O_{39}(Sn\text{-}n\text{-}C_4H_9)]^{4-}$, and $[PW_{11}O_{39}(Sn\text{-}OH)]^{4-}$. In addition, the pore size distributions, which ranged from the microporous to mesoporous, and the external surface areas were determined by combining Ar porosimetry with conventional mesopore analysis using N_2 adsorption-desorption isotherms. These Cs salts had highly developed micropores with small external surface areas, regardless of the presence or absence of functional groups (*n*-butyl and hydroxyl). We discuss the mechanism for the formation of micropores in terms of the crystal structures and morphology of the particles and in comparison with that for $Cs_3[PW_{12}O_{40}]$. In addition, the effects of *n*-butyl and hydroxyl groups on the adsorption properties were investigated by measuring the adsorption isotherms of various adsorbates.

(Fig. 1)

2. Experimental

2.1 Synthesis of Cs and K salts of polyoxotungstates

2.1.1 Materials

Dodecatungstophosphoric acid ($H_3PW_{12}O_{40}\cdot nH_2O$) and dodecatungstosilicic acid

($H_4SiW_{12}O_{40}\cdot nH_2O$) were supplied by Nippon Inorganic Color and Chemical Co. After $H_3PW_{12}O_{40}\cdot nH_2O$ was recrystallized from water several times, $H_3PW_{12}O_{40}\cdot nH_2O$ was dried at 338 K in a vacuum to obtain $H_3PW_{12}O_{40}\cdot 6H_2O$. $H_4SiW_{12}O_{40}\cdot nH_2O$ was dried in a similar manner to $H_3PW_{12}O_{40}\cdot 6H_2O$, but recrystallization was not conducted before drying.

n-$C_4H_9SnCl_3$ (Aldrich), $SnCl_2\cdot 2H_2O$ (Wako Pure Chemical Co., Ltd.), CsCl (Wako Pure Chemical Co., Ltd.), Cs_2CO_3 (Aldrich), $KHCO_3$ (Wako Pure Chemical Co., Ltd.), KCl (Wako Pure Chemical Co., Ltd.), and bromine water (Wako Pure Chemical Co., Ltd.) were used as received.

2.1.2 Synthesis of a Cs salt of $[PW_{11}O_{39}(Sn\text{-}n\text{-}C_4H_9)]^{4-}$ (**Cs_4-PW11(Sn-*n*-Bu)**)

To an aqueous solution of $H_3PW_{12}O_{40}$ (6.0×10^{-2} mol dm^{-3}, 100 cm^3), 1 g of KCl was added, and the pH of the solution was adjusted to 5.4 with an aqueous solution of $KHCO_3$ (1 mol dm^{-3}). The insoluble matter was filtered off. The filtrate was concentrated under vacuum until a solid just started to form and then was allowed to stand overnight. The resulting white solid ($K_7[PW_{11}O_{39}]\cdot 15H_2O$, **$K_7$-PW11**) was recovered by filtration and dried at room temperature overnight.

$[PW_{11}O_{39}(Sn\text{-}n\text{-}C_4H_9)]^{4-}$ was prepared according to the method in [40] with some modifications. Liquid *n*-$C_4H_9SnCl_3$ (300 μL, 1.756 mmol) was added to an aqueous solution (100

cm^3) of 1.55 mmol of **K_7-PW11** with stirring. The solution was stirred at room temperature for 1 h to yield $[PW_{11}O_{39}(Sn\text{-}n\text{-}C_4H_9)]^{4-}$ in solution. Incorporation of n-C_4H_9 group was confirmed from ^1H NMR spectrum of $[PW_{11}O_{39}(Sn\text{-}n\text{-}C_4H_9)]^{4-}$ in D_2O (see Fig. S1, Supplementary information). After the insoluble matter was filtered off, an aqueous solution of CsCl (0.5 mol dm^{-3}, 15 cm^3) was added to the resulting filtrate. The clear solution changed to a white colloidal suspension just after the addition of the CsCl solution. The suspension was then allowed to stand overnight at room temperature. The resulting white solid was recovered by filtration and dried at room temperature overnight. The solid was suspended in water (100 cm^3), and the suspension was heated at 368 K until most of the solid dissolved. After the insoluble matter was filtered off at 368 K, the filtrate was cooled and allowed to stand at room temperature overnight, during which time a solid precipitated. The solid was collected by filtration and dried under ambient conditions, yielding $Cs_4[PW_{11}O_{39}(Sn\text{-}n\text{-}C_4H_9)]\cdot 8H_2O$, hereafter referred to as **Cs_4-PW11(Sn-*n*-Bu)**. Yield: 59%. ^{31}P MAS NMR: δ (ppm) –12.4. IR (KBr, cm^{-1}): ν 2960 (w), 2931 (w), 2871 (w), 1069 (m), 971 (s), 879 (m), 798 (s). Elemental analysis for $Cs_4[PW_{11}O_{39}(Sn\text{-}n\text{-}C_4H_9)]\cdot 8H_2O$ (%): calcd P 0.88; W 57.3; Sn 3.36; Cs 15.1; C 1.36; H 0.71; found P 0.79; W 57.6; Sn 3.06; Cs 14.8; C 1.40; H 0.68.

*2.1.3 Synthesis of a Cs salt of $[PW_{11}O_{39}(Sn\text{-}OH)]^{4-}$ (**Cs_4-PW11(Sn-OH)**)*

$K_5[PW_{11}O_{39}Sn]\cdot 4H_2O$ was prepared by a similar manner to [41], but using $SnCl_2\cdot 2H_2O$ and water as a tin compound and solvent, respectively, instead of $SnSO_4$ and an aqueous solution of acetic acid. **K_7-PW11** (10 g, 3.13 mmol) was suspended in water (80 cm^3), and then the suspension was heated at 353 K until all of the solid dissolved. Nitrogen gas was bubbled into the solution at 353 K for 1 h, and then $SnCl_2\cdot 2H_2O$ (0.73 g, 3.15 mmol) was added. The solution was stirred at 353 K overnight with the continuous N_2 bubbling. After the insoluble matter was filtered off, the resulting dark-green solution was concentrated in a vacuum at 318 K until a solid began to form. The solution containing a small amount of the solid was allowed to stand at room temperature overnight. The resulting yellow solid ($K_5[PW_{11}O_{39}Sn]\cdot 4H_2O$) was collected by filtration, washed with water, and then dried at 333 K overnight.

The powder of $K_5[PW_{11}O_{39}Sn]\cdot 4H_2O$ (5.0 g, 1.63 mmol) was dissolved in water (50 cm^3). To the solution, bromine water (10 cm^3) was added [41], during which time the color of the solution momentarily changed from light yellow to clear, affording $[PW_{11}O_{39}(Sn\text{-}OH)]^{4-}$. Air was bubbled into the solution for 1 h to remove unreacted Br_2. An aqueous solution of CsCl (1 mol dm^{-3}, 9.97 cm^3) was added dropwise to the solution. The resulting suspension was allowed to stand at room temperature for 24 h. The white solid was collected by filtration, washed with water, and dried at 373 K overnight to afford $Cs_{3.6}K_{0.4}[PW_{11}O_{39}(Sn\text{-}OH)]\cdot 8H_2O$, hereafter referred to as

Cs_4-PW11(Sn-OH). Yield: 91%. ^{31}P MAS NMR: δ(ppm) –12.2. IR (KBr, cm^{-1}): ν 1083 (m), 1055 (m), 982 (s), 883 (m), 800 (s). Elemental analysis for $Cs_{3.6}K_{0.4}[PW_{11}O_{39}(Sn\text{-}OH)]\cdot 8H_2O$ (%): calcd P 0.90; W 58.6; Sn 3.44; Cs 13.9; K 0.45; found P 0.91; W 58.6; Sn 3.57; Cs 13.9; K 0.45.

*2.1.4 Synthesis of $Cs_3[PW_{12}O_{40}]$ (**Cs_3-PW12**) and $Cs_4[SiW_{12}O_{40}]$ (**Cs_4-SiW12**)*

An aqueous solution of Cs_2CO_3 (0.10 mol dm^{-3}, 24 cm^3) was added dropwise to an aqueous solution of $H_3[PW_{12}O_{40}]$ (8.0×10^{-2} mol dm^{-3}, 20 cm^3) with stirring. A white suspension formed. After the suspension was stirred for 30 min, it was allowed to stand for 48 h at room temperature. The suspension was completely dried at 313 K in a vacuum to afford a white solid. Finally, the white solid was dried in a vacuum at room temperature to obtain $Cs_3[PW_{12}O_{40}]\cdot 6H_2O$ (**Cs_3-PW12**). Yield: 100%. ^{31}P MAS NMR: δ(ppm) –15.0. IR (KBr, cm^{-1}): ν 1080 (m), 985 (s), 890 (m), 804 (s). Elemental analysis for $Cs_3[PW_{12}O_{40}]\cdot 6H_2O$ (%): calcd P 0.92; W 65.2; Cs 11.8; found P 0.92; W 65.1; Cs 11.6.

$Cs_4[SiW_{12}O_{40}]\cdot 9H_2O$ (**Cs_4-SiW12**) was prepared in a similar manner to that for **Cs_3-PW12** using an aqueous solution of $H_4[SiW_{12}O_{40}]$ instead of $H_3[PW_{12}O_{40}]$. Yield: 100%. IR (KBr, cm^{-1}): ν 980 (m), 926 (s), 878 (w), 779 (s). Elemental analysis for $Cs_4[SiW_{12}O_{40}]\cdot 9H_2O$ (%): calcd Si 0.80; W 61.8; Cs 14.9; found Si 0.86; W 61.6; Cs 14.8.

2.2 Characterization

^{31}P nuclear magnetic resonance (NMR) spectra were acquired at ambient temperature on a JEOL EX-400 NMR spectrometer. The samples were dissolved into H_2O/D_2O (5:1 v/v). Chemical shifts were referenced to the external standard 85% H_3PO_4 (0 ppm). Solid-state ^{31}P magic angle spinning (MAS) NMR spectra were acquired on a JEOL ECA-400 spectrometer. The spinning rate of the sample was 7.0 kHz. A $\pi/2$ pulse width of 5.5 μs and a pulse delay of 5 s were used. 85% H_3PO_4 was used as a reference.

Thermogravimetric/differential thermal analysis (TG/DTA) was conducted in air on a Rigaku Thermo plus 8120. Temperature of the sample was increased at a rate of 10 K min^{-1}. Infrared (IR) spectra of the samples were recorded on an IR spectrometer (FT-IR/230, JASCO) as KBr (Merck) pellets diluted to 0.5 wt%. Powder X-ray diffraction (XRD) was performed using an X-ray diffractometer (Rigaku Mini Flex) with Cu Kα radiation (λ = 0.154 nm).

Adsorption-desorption isotherms of N_2 at 77 K were acquired on a Belsorp-mini instrument (BEL Japan Inc.) after the samples were pretreated at 473 K in a N_2 flow for 1 h. Specific surface areas were estimated from the slopes of the *t*-plots derived from the N_2 adsorption isotherms. Mesopore-size distributions were calculated by using the Dollimore-Heal (DH) method on the

desorption isotherms of N_2. Micropore-size distributions were determined by using the Saito-Foley method on Ar adsorption isotherms at 87 K measured on an automatic apparatus (Belsorp 28SA, BEL Japan Inc.). Before measurement, the samples were pretreated at 473 K in a vacuum for 3 h.

Elemental analyses of the compounds were performed on an atomic absorption spectrometer (HITACHI A-2000) for Cs and K and inductively coupled plasma-atomic emission spectrometer (Shimadzu ICPS-7000) for P, W, and Sn. The amounts of C and H of the compounds were determined by the Center for Instrumental Analysis at Hokkaido University (Sapporo, Japan).

Adsorption isotherms of H_2O, methanol, ethanol, 1-propanol, *n*-hexane, and benzene were obtained at 298 K on an automatic apparatus (Belsorp 18, BEL Japan Inc.) after the samples were pretreated at 473 K in a vacuum for 3 h.

3. Results and discussion

3.1 Structures of Keggin-POMs in solution and of their Cs salts

We investigated the formation of the heteropoly anions $[PW_{11}O_{39}(Sn\text{-}n\text{-}C_4H_9)]^{4-}$ and $[PW_{11}O_{39}(Sn\text{-}OH)]^{4-}$ in solution. Figure 2A shows ^{31}P NMR spectra of $[PW_{12}O_{40}]^{3-}$, $[PW_{11}O_{39}]^{7-}$, $[PW_{11}O_{39}(Sn\text{-}n\text{-}C_4H_9)]^{4-}$, and $[PW_{11}O_{39}(Sn\text{-}OH)]^{4-}$ in H_2O/D_2O. In the ^{31}P NMR spectrum of

$[PW_{12}O_{40}]^{3-}$, there was a peak at –14.7 ppm (Fig. 2A(a)), which is the same as the value previously reported [42]. When one $[W=O]^{4+}$ was eliminated from $[PW_{12}O_{40}]^{3-}$ to form a mono-lacunary $[PW_{11}O_{39}]^{7-}$, the ^{31}P NMR peak shifted to –10.5 ppm (Fig. 2A(b)), which is also consistent with the previously reported chemical shift [42]. For the *Keggin-POM* with an *n*-butyl group ($[PW_{11}O_{39}(Sn\text{-}n\text{-}C_4H_9)]^{4-}$), only one peak was observed, indicating that there was no phosphorus-containing impurities (Fig. 2A(c)). The ^{31}P NMR chemical shift for $[PW_{11}O_{39}(Sn\text{-}n\text{-}C_4H_9)]^{4-}$ (–11.9 ppm) is similar to that for $[PW_{11}O_{39}Sn]^{5-}$ (see Fig. S2(A) in Supplementary information), in which Sn^{2+} was incorporated into the lacunal sites of $[PW_{11}O_{39}]^{7-}$ [41]. In other words, $[Sn\text{-}n\text{-}C_4H_9]^{3+}$ could be incorporated into the lacunal sites of $[PW_{11}O_{39}]^{7-}$ to form $[PW_{11}O_{39}(Sn\text{-}n\text{-}C_4H_9)]^{4-}$. The incorporation of Sn-*n*-C_4H_9 was also confirmed from 1H NMR spectrum of $[PW_{11}O_{39}(Sn\text{-}n\text{-}C_4H_9)]^{4-}$ in D_2O. The chemical shift (–11.9 ppm) for $[PW_{11}O_{39}(Sn\text{-}OH)]^{4-}$ (Fig. 2A(d)) is the same as that for $[PW_{11}O_{39}(Sn\text{-}n\text{-}C_4H_9)]^{4-}$, indicating that $[Sn\text{-}OH]^{3+}$ could be introduced into the lacunal sites of $[PW_{11}O_{39}]^{7-}$ as $[PW_{11}O_{39}(Sn\text{-}n\text{-}C_4H_9)]^{4-}$. Since the chemical shift was changed from –12.4 ppm for $[PW_{11}O_{39}Sn]^{5-}$ into –11.9 ppm for $[PW_{11}O_{39}(Sn\text{-}OH)]^{4-}$ by the treatment with bromine water, Sn^{2+} incorporated in $[PW_{11}O_{39}Sn]^{5-}$ was successfully oxidized.

Figure 2B shows solid-state ^{31}P MAS NMR spectra of **Cs_3-PW12**, **Cs_4-PW11(Sn-*n*-Bu)**, and

Cs_4-PW11(Sn-OH), which were obtained by reacting Cs^+ with $[PW_{12}O_{40}]^{3-}$, $[PW_{11}O_{39}(Sn\text{-}n\text{-}C_4H_9)]^{4-}$, and $[PW_{11}O_{39}(Sn\text{-}OH)]^{4-}$, respectively, in the corresponding aqueous solutions. The ^{31}P NMR chemical shifts for the three Cs salts are basically the same as those in the corresponding solutions, as shown in Fig. 2A. In addition, each Cs salt gave only one peak, indicating that no decomposition and no reconstruction of the heteropoly anions occurred during the formation of the Cs salts.

IR spectra of **Cs_3-PW12**, **K_7-PW11**, **Cs_4-PW11(Sn-*n*-Bu)**, **Cs_4-PW11(Sn-OH)**, and **Cs_4-SiW12** are shown in Fig. 3. In the IR spectra of **Cs_3-PW12**, there were four IR bands at 1080, 985, 890, and 804 cm^{-1}, which were assigned as ν_{as}(P-O), ν_{as}(W=O), ν_{as}(W-O-W), and ν_{as}(W-O-W) for Keggin-type $[PW_{12}O_{40}]^{3-}$ (Fig. 3a) [42]. In the IR spectrum for the mono-lacunal heteropoly anion **K_7-PW11**, ν_{as}(P-O) was split into two bands at 1086 and 1042 cm^{-1}, and the band due to ν_{as}(W-O-W) was split into several bands (Fig. 3b) because the symmetry of the heteropoly anion changed from T_d to C_s [42]. On the other hand, the IR spectrum of **Cs_4-PW11(Sn-*n*-Bu)** (Fig. 3c) is similar to that of **Cs_3-PW12**, clearly indicating that the heteropoly anion in **Cs_4-PW11(Sn-*n*-Bu)** has T_d symmetry. In other words, $[Sn\text{-}n\text{-}C_4H_9]^{3+}$ was incorporated into the lacunal site of $[PW_{11}O_{39}]^{7-}$, forming a complete *Keggin-POM*. The IR bands for CH_3 and CH_2 stretching were only observed for **Cs_4-PW11(Sn-*n*-Bu)** in the range of 2800–3000cm^{-1}. The IR spectrum for

Cs_4-PW11(Sn-OH) is similar to that for **Cs_4-PW11(Sn-*n*-Bu)**, except that ν_{as}(P-O) was split into two bands. Since $[Sn\text{-}OH]^{3+}$ was incorporated into the lacunal site of $[PW_{11}O_{39}]^{7-}$ on the basis of the ^{31}P MAS NMR spectrum (Fig. 2g), the splitting of the IR band was not due to the presence of impurities like $[PW_{11}O_{39}]^{7-}$. In fact, the IR spectra for **Cs_4-PW11(Sn-OH),** except for the ν_{as}(P-O) bands, are different from those for **K_7-PW11**. Although the ionic radius of the Sn^{4+} ion (r_{Sn4+} = 0.055 nm) is close to that of the W^{6+} ion (r_{W6+} = 0.060 nm), that of a Sn^{4+} ion coordinated by a OH group is probably much smaller than that of a bare Sn^{4+} ion due to the electron withdrawing character of the OH group. This would result in the deformation of the Keggin unit from pure T_d symmetry, leading to the splitting of the ν_{as}(P-O) bands. For **Cs_4-SiW12**, four bands due to the Keggin structure were observed at 980, 926, 878, and 779 cm^{-1}, which were assigned as ν_{as}(W=O), ν_{as}(Si-O), ν_{as}(W-O-W), and ν_{as}(W-O-W), respectively [42].

Fig. 4 shows TG-DTA profiles for **Cs_3-PW12**, **Cs_4-PW11(Sn-*n*-Bu)**, **Cs_4-PW11(Sn-OH)**, and **Cs_4-SiW12** in air. Weight loss due to desorption of water was observed in the range of 300–380 K. An exothermic weight loss of 1.21 wt% in the temperature range of 550–780 K was only observed for **Cs_4-PW11(Sn-*n*-Bu)**, which was due to the combustion of the *n*-butyl group. This result indicates that **Cs_4-PW11(Sn-*n*-Bu)** is stable in air up to 550 K.

Table 1 summarizes the elemental analysis data for **Cs_3-PW12**, **Cs_4-SiW12**,

Cs_4-PW11(Sn-*n*-Bu), and **Cs_4-PW11(Sn-OH)**. The figures in parenthesis in Table 1 are the weight percent of each element calculated from the chemical formulae shown in the rightmost column of Table 1. The numbers of crystalline waters were estimated from the weight loss observed in the TG profiles below 403 K. For each Cs salt, the elemental analysis data were consistent with the values calculated from the formula. On the basis of the elemental analysis and ^{31}P NMR and IR spectra, it was concluded that the Cs salts of the tetravalent *Keggin-POM* with *n*-butyl and hydroxyl groups could be synthesized.

Powder XRD patterns for **Cs_3-PW12**, **Cs_4-SiW12**, **Cs_4-PW11(Sn-*n*-Bu)**, and **Cs_4-PW11(Sn-OH)** are shown in Fig. 5. The XRD pattern for **Cs_3-PW12** (Fig. 5a) was assigned to a body-centered cubic (bcc) structure [26]. The XRD pattern for **Cs_4-SiW12**, which has a bcc structure [31] (Fig. 5b), is similar to that for **Cs_3-PW12**, although the diffraction lines were very sharp and intense in comparison to **Cs_3-PW12**, indicating that the crystallites of **Cs_4-SiW12** are large. It should be noted that **Cs_4-PW11(Sn-*n*-Bu)** (Fig. 5c) and **Cs_4-PW11(Sn-OH)** (Fig. 5d) also show XRD patterns consistent with a bcc structure, and the diffraction angles for **Cs_4-PW11(Sn-*n*-Bu)** and **Cs_4-PW11(Sn-OH)** are almost the same as those for **Cs_4-SiW12**. The XRD patterns clearly showed that the crystalline structures of the four Cs salts were basically the same regardless of the charges of the anion (–3 or –4) and the presence or absence of functional

groups (*n*-butyl and hydroxyl groups).

From the diffraction lines, the lattice constants (*a*) were calculated to be 1.182, 1.178, 1.179, and 1.180 nm for **Cs_3-PW12**, **Cs_4-SiW12**, **Cs_4-PW11(Sn-*n*-Bu)**, and **Cs_4-PW11(Sn-OH)**, respectively (Table 2). The crystallite sizes were estimated from the diffraction line at around 2θ = 26.1° to be 11.7, 45.3, 50.9, and 34.0 nm for **Cs_3-PW12**, **Cs_4-SiW12**, **Cs_4-PW11(Sn-*n*-Bu)**, and **Cs_4-PW11(Sn-OH)**, respectively (Table 2). It should be noted that the crystallite sizes for the Cs salts of tetravalent *Keggin-POMs* are much larger than that for **Cs_3-PW12**.

3.2 Surface areas, porosities, and pore structures of Cs salts

Fig. 6 shows adsorption-desorption isotherms of N_2 at 77 K for **Cs_3-PW12**, **Cs_4-SiW12**, **Cs_4-PW11(Sn-*n*-Bu)**, and **Cs_4-PW11(Sn-OH)**. The insets in Fig. 6 are *t*-plots calculated from the corresponding adsorption isotherms. For each Cs salt, a steep increase in the adsorption amounts at low-pressure (P/P_0 < 0.05) was observed, suggesting the presence of micropores. Only **Cs_3-PW12** gave a type IV isotherm (Fig. 6a), indicating that this material had mesopores. Okuhara et al. have reported that $Cs_3PW_{12}O_{40}$, prepared by using a similar procedure to that used in the present study, is a porous material having both micropores and mesopores and that the mesopores are *ca*. 4 nm in size [29,30]. The results shown in Fig. 6a are consistent with previous

reports [29,30]. On the other hand, **Cs_4-SiW12**, **Cs_4-PW11(Sn-*n*-Bu)**, and **Cs_4-PW11(Sn-OH)** gave type I isotherms. In addition, N_2 uptakes in the range of $0.1 < P/P_0 < 0.8$ were small, indicating that they have small external surface areas.

The total and external surface areas were estimated from the slopes of the *t*-plots and are summarized in Table 2. Although the total surface area of **Cs_3-PW12** was 138 m^2 g^{-1}, 73% of it is the external surface area (100 m^2 g^{-1}). This is consistent with the fact that **Cs_3-PW12** has pores with bimodal distributions. The total surface area of **Cs_4-SiW12** was large (168 m^2 g^{-1}), but its external surface area was small (8 m^2 g^{-1}), the value of which corresponds to less than 5% of the total surface area. The total surface areas of **Cs_4-PW11(Sn-*n*-Bu)** and **Cs_4-PW11(Sn-OH)** were 208 and 177 m^2 g^{-1}, respectively, which are comparable to that of **Cs_4-SiW12**. In addition, the ratios of the external to the total surface areas were 2% and 6% for **Cs_4-PW11(Sn-*n*-Bu)** and **Cs_4-PW11(Sn-OH)**, respectively, indicating that their micropores are highly-developed.

Fig. 7 shows pore-size distributions of the micropores and mesopores for **Cs_3-PW12**, **Cs_4-SiW12**, **Cs_4-PW11(Sn-*n*-Bu)**, and **Cs_4-PW11(Sn-OH)**. In the micropore-size distribution for **Cs_3-PW12**, an intense peak at 0.56 nm and a broad shoulder in the range of 0.7–0.9 nm were observed. In addition, a large peak in the range of 3–5 nm was present in the mesopore region. The micropore-size distributions of the Cs salts of tetravalent *Keggin-POMs*, including **Cs_4-SiW12**,

Cs_4-PW11(Sn-*n*-Bu), and **Cs_4-PW11(Sn-OH)**, which showed sharp peaks at 0.59 nm and shoulders at 0.62 nm in the micropore region and only a little peak in the mesopore region, are very similar to each other.

For the microporous Cs salts (**Cs_4-SiW_{12}**, **Cs_4-PW_{11}(Sn-*n*-Bu)**, and **Cs_4-PW_{11}(Sn-OH)**), the micropore volumes (V_{Micro}: $cm^3\ g^{-1}$) were estimated by applying the following equation to the intercept (I: $cm^3\ g^{-1}$) of line B in the *t*-plot shown in the inset of Fig. 6:

$$V_{Micro} = \frac{I}{C} \times \frac{M}{\rho} \qquad (1)$$

where, M, C, and ρ are the molecular weight of N_2 (28.01 g mol^{-1}), the volume of an ideal gas per mole (22.4×10^3 $cm^3\ mol^{-1}$), and the density of liquid N_2 at 77 K (0.808 g cm^{-3}), respectively. The micropore volumes for **Cs_4-SiW12**, **Cs_4-PW11(Sn-*n*-Bu)**, and **Cs_4-PW11(Sn-OH)** were 0.056, 0.074, and 0.055 $cm^3\ g^{-1}$, respectively (Table 2).

As shown in Fig. 5, the four Cs salts have the same bcc structure, and the lattice constants are similar to each other regardless of the charges of the anions (Table 2). However, the size distributions of the micropores in the Cs salts of the trivalent *Keggin-POM* **Cs_3-PW12** and those for tetravalent *Keggin-POMs* **Cs_4-SiW12**, **Cs_4-PW11(Sn-*n*-Bu)**, and **Cs_4-PW11(Sn-OH)** are different. This suggests that the formation mechanisms for the micopores in the former and latter Cs salts are different. Misono and Mizuno have reported that $Cs_3PW_{12}O_{40}$ has no intrinsic micopores in the

crystal lattice since the BET surface area of $Cs_3PW_{12}O_{40}$, estimated from the adsorption isotherm of N_2 is consistent with the surface area of the outer surface of the $Cs_3PW_{12}O_{40}$ particles, which was calculated from the real density of $Cs_3PW_{12}O_{40}$ and the particle size estimated from TEM images [42]. Okuhara and co-workers have proposed a model in which the micropores of the Cs salts of $[PW_{12}O_{40}]^{3-}$, like $Cs_3PW_{12}O_{40}$, are the intercrystallite spaces formed at crystallographic mismatches between the crystal faces of the microcrystallites [26,27,29]. As shown in Table 2, in the case of **Cs_3-PW12**, the total surface area (136 $m^2\ g^{-1}$), which was estimated from N_2 adsorption isotherms, is actually close to the surface area of the outer surface (S_{os}: $m^2\ g^{-1}$), calculated from the real density and crystallite size estimated from the XRD pattern by using:

$$S_{OS} = \frac{6000}{\rho \times d} \qquad (2)$$

where ρ and d are the real density of $Cs_3PW_{12}O_{40}$ (6.5 g cm^{-3}) and the crystallite size (nm) estimated from the XRD line at ~26.1º by using Scherrer's equation, respectively.

For **Cs_4-SiW12**, we calculated S_{OS} by using a method similar to that for **Cs_3-PW12** (Table 2). S_{OS} of **Cs_4-SiW12** was calculated to be 20 $m^2\ g^{-1}$. However, this value is significantly smaller than the actual surface area (168 $m^2\ g^{-1}$) estimated from the N_2 adsorption isotherm. This large difference can be explained if micropores are present inside the crystallites of **Cs_4-SiW12**, unlike **Cs_3-PW12**. For **Cs_4-PW11(Sn-*n*-Bu)** and **Cs_4-PW11(Sn-OH)**, S_{OS} were 18 and 27 $m^2\ g^{-1}$,

respectively, which are much smaller than the actual surface areas (Table 2), suggesting that both **Cs_4-PW11(Sn-*n*-Bu)** and **Cs_4-PW11(Sn-OH)** have micropores inside the crystallites, like **Cs_4-SiW12**.

In the bcc structure, heteropoly anions can be located in the center and at each corner of the unit cell, and Cs^+ ions are located between two heteropoly anions (Fig. 8). To construct the bcc structure, the ratio of the cations (Cs^+) to the heteropoly anions must be three. In the case of **Cs_3-PW12**, the ratio of Cs^+/(heteropoly anion) required to achieve charge balance was three due to the trivalent *Keggin-POM* and is consistent with that required for a bcc structure. In other words, all of the cation and anion sites are occupied with Cs^+ and $[PW_{12}O_{40}]^{3-}$ ions, respectively (Fig. 8A). However, for the Cs salts of the tetravalent *Keggin-POMs*, the ratio of Cs^+/(heteropoly anion) was four, which is necessary in order to achieve charge balance. Thus, the ratio of Cs^+/(heteropoly anion) is not consistent with that required for a bcc structure, which is three. If a quarter of the heteropoly anions are defective in the Cs salts of the tetravalent *Keggin-POMs*, i.e., anion vacancies are present in the crystallites (Fig. 8B), the Cs^+-heteropoly anion mismatch can be avoided. Therefore, we speculate that anion vacancies are the origins of the micropores. Schlögl and co-workers have proposed a similar model for the micropores in the crystallites of $Cs_4[PMo_{11}VO_{40}]\cdot 5H_2O$ [19].

On the basis of the anion vacancy model, we calculated the number of anion vacancies per unit weight of the Cs salt by using:

$$N_{defect} = \frac{N_A}{3 \times F_W} \quad (3)$$

where N_{defect}, F_W, and N_A are the number of the anion vacancies per unit weight of the Cs salt (g^{-1}), the formula weight of the Cs salt, and Avogadro's number, respectively. If the heteropoly anion is a sphere with a diameter of 1.1 nm [44], the total volume of the anion vacancies per unit weight of the Cs salt (V_{defect}, $cm^3\ g^{-1}$) can be calculated by using:

$$V_{defect} = N_{defect} \times (7.0 \times 10^{-22}) \quad (4)$$

where the constant 7.0×10^{-22} (cm^3) is the volume of one *Keggin-POM*. V_{defect} was calculated to be 0.041 $cm^3\ g^{-1}$ for **Cs_4-SiW12** (Table 2). This value is consistent with the micropore volume estimated from the N_2 adsorption isotherms (0.056 $cm^3\ g^{-1}$, Table 2). In addition, V_{defect} for **Cs_4-PW11(Sn-*n*-Bu)** and **Cs_4-PW11(Sn-OH)** are consistent with the micropore volumes. For all microporous Cs salts, the micropore volumes estimated from the N_2 adsorption isotherms are slightly larger than the corresponding V_{defect}. We think that the N_2 adsorption method determines the spaces connecting the anion vacancies, into which N_2 can approach from the outside of the crystallite. Thus, the micropore volumes estimated from N_2 adsorption isotherms are larger than V_{defect}.

3.2 Adsorption properties of the microporous Cs salts

As discussed in 3.1, *n*-butyl groups were introduced into *Keggin-POM* to afford **Cs_4-PW11(Sn-*n*-Bu)**. However, we believe that only a part of the *n*-butyl groups is exposed on the surface. In other words, some of them are directed away from the micropores. Thus, we estimated the number of *n*-butyl groups exposed on the surface as follows. The Sn-C_4H_9 bond in **Cs_4-PW11(Sn-*n*-Bu)** was hydrolyzed by heating it in a He flow containing H_2O vapor (3.3 kPa) at 473 K for 6 h, and we compared the carbon contents of the samples before and after the treatment to estimate the number of -C_4H_9 groups exposed on the micropores. Before treatment, **Cs_4-PW11(Sn-*n*-Bu)** had a carbon content of 1.56 wt%, which corresponds to 0.324 mmol g^{-1} being *n*-butyl groups, and after treatment, the carbon content was 1.23 wt%, indicating that 21% of the *n*-butyl groups were eliminated by using the treatment. This result suggested that 21% of *n*-butyl groups were exposed on the surface. The crystalline structure was not changed during the treatment, and the micropore was also retained even after the treatment (see Fig. S3 in Supplementary information). In a separate experiment, it was confirmed that the carbon content did not decrease further with an increase in the treatment time under the present conditions. As discussed in section 3.1, a quarter of the heteropoly anions in **Cs_4-PW11(Sn-*n*-Bu)** have defects,

which form the micropores. If it is assumed that the heteropoly anions are arranged in a parallel manner within the crystallite, the heteropoly anions in which *n*-butyl groups directed towards the micropores are a quarter of the total heteropoly anions, which roughly corresponds to the fraction of the *n*-butyl groups exposed on the surface.

In addition, for **Cs_4-PW11(Sn-OH)**, we estimated the fraction of hydroxyl groups exposed on the surface by using a method similar to that for estimating the amount of the *n*-butyl groups exposed on the surface, except that chlorotrimethylsilane ($ClSiMe_3$) was used instead of H_2O. **Cs_4-PW11(Sn-OH)** was treated under a He flow containing an excess amount of $ClSiMe_3$ at 473 K for 6 h to convert only the Sn-OH groups exposed on the surface to Sn-O-$SiMe_3$. After treatment, the carbon content was 0.24 wt%, which corresponded to an $SiMe_3$ content of 0.067 mmol g^{-1}. Introduction of -$SiMe_3$ was also confirmed by ^{29}Si MAS NMR (see Fig. S4 in Supplementary information). The crystalline structure was not changed by the treatment and the micropore volume was decreased due to the introduction of -$SiMe_3$ groups (see Fig. S5 in Supplementary information). Since the total number of Sn-OH groups in the untreated **Cs_4-PW11(Sn-OH)** was 0.29 mmol g^{-1}, 23% of the hydroxyl groups were exposed on the surface. This value is similar to that of the *n*-butyl groups exposed on the surface.

Fig. 9 shows a comparison of the adsorption isotherms of water, primary alcohols (C_1-C_3),

benzene and *n*-hexane at 298 K on microporous **Cs_4-SiW12**, **Cs_4-PW11(Sn-*n*-Bu)**, and **Cs_4-PW11(Sn-OH)**. The adsorption amounts per unit surface area are plotted in Fig. 9, making it possible to ignore the differences in the surface areas. The *n*-butyl groups had a big effect on the adsorption of the water. As shown in Fig. 9a, the amount of water adsorbed at P = 2 Torr on **Cs_4-SiW12** was 0.14 cm^3 m^{-2}, whereas that on **Cs_4-PW11(Sn-*n*-Bu)** was only one-third of that on **Cs_4-SiW12**. Since the adsorption amounts at nearly the saturated vapor pressure (P/P_0 = 0.95) are similar to each other, it seems unlikely that the difference in the low-pressure region is due to the difference in the micropore volumes. Thus, the difference in the hydrophobicity is a plausible explanation for the different amounts of H_2O adsorbed. It has been reported that the surfaces of the Cs salts of Keggin-type heteropolyacids, like $Cs_{2.5}H_{0.5}[PW_{12}O_{40}]$, are rather hydrophobic [45]. The H_2O adsorption isotherms clearly showed that the introduction of *n*-butyl groups into the *Keggin-POM* increased the hydrophobicity.

The surface density of the *n*-butyl groups on **Cs_4-PW11(Sn-*n*-Bu)** was estimated from the surface area and the number of *n*-butyl groups exposed on the surface to be only 0.20 nm^{-2}. In other words, only one *n*-butyl group was present per 5.0 nm^2 of the surface. This surface area is extremely large in comparison with the cross-sectional area of adsorbed water (0.125 nm^2). In other words, the *n*-butyl groups greatly affect the hydrophobicity of the surface despite the low

surface density. Inumaru et al. have demonstrated by using ^{13}C MAS NMR that *n*-alkyl groups (C8 and C5) grafted on the surface of mesoporous silica are highly mobile near room temperature [46]. Thus, we concluded that the *n*-butyl groups on the surface of **Cs_4-PW11(Sn-*n*-Bu)** were active like the *n*-alkyl groups on the mesoporous silica. Considering the length (~0.7 nm) and the active movement of the *n*-butyl groups, it is likely that they affect the hydrophobicity of the surface of **Cs_4-PW11(Sn-*n*-Bu)**, although the surface density was low (Fig. 10A). On the other hand, the OH groups present on the surface of **Cs_4-PW11(Sn-OH)** have little impact on the adsorption properties, although the surface density was almost the same as that for the *n*-butyl groups in **Cs_4-PW11(Sn-*n*-Bu)**. In fact, the adsorption isotherms of various adsorbates on **Cs_4-PW11(Sn-OH)**, except for 1-propanol and benzene, which preferentially adsorbed on **Cs_4-PW11(Sn-OH)**, are similar to those on **Cs_4-SiW12** (Fig. 9). Since the hydroxyl groups are short, they have less impact on the adsorption properties (Fig. 10B).

Although there were no differences among the adsorption isotherms of *n*-hexane on the Cs salts, there were considerable differences in the adsorption isotherms of benzene on **Cs_4-PW11(Sn-*n*-Bu)**, **Cs_4-PW11(Sn-OH)**, and **Cs_4-SiW12**. Since the interactions between the C-H moieties of saturated hydrocarbons and aromatic compounds, i.e., -CH$\cdots\pi$ interactions, are extremely weak [47, 48], it is reasonable that the adsorbability of benzene onto the surface of

Cs_4-PW11(Sn-*n*-Bu) is low, meaning that benzene is not included in the micropores of **Cs_4-PW11(Sn-*n*-Bu)**. In contrast, **Cs_4-PW11(Sn-OH)** adsorbed benzene strongly, as indicated by the steep increase in the amount of benzene adsorbed at low pressure (Fig. 9). It has been reported that a weak -OH···π hydrogen bond can occur [47]. In general hydrogen bonds are not strong; however, they would explain preferential adsorption of benzene in the micropores of **Cs_4-PW11(Sn-OH)**. For the adsorption isotherms of C_2H_5OH, there was a large difference in the adsorption amount between **Cs_4-SiW12** and **Cs_4-PW11(Sn-*n*-Bu)** at low pressure (P < 3 Torr). However, the difference in the adsorption amounts was a little for C_3H_7OH. This is probably due to lower polarity of C_3H_7OH than C_2H_5OH.

4. Conclusions

Neutral Cs salts of the tetravalent *Keggin-POMs* $Cs_4[SiW_{12}O_{40}]$, $Cs_4[PW_{11}O_{39}(Sn\text{-}n\text{-}C_4H_9)]$, and $Cs_4[PW_{11}O_{39}(Sn\text{-}OH)]$ were synthesized, and their molecular, crystalline, and pore structures were investigated. All of the Cs salts formed ionic crystals with similar body-centered cubic structures to that of a Cs salt of a trivalent *Keggin-POM*, $Cs_3[PW_{12}O_{40}]$. The crystalline structures of the Cs salts were similar to each other regardless of the presence or absence of functional groups (*n*-butyl and hydroxyl) and the charges of the anions (–3 or –4). The Cs salts of the tetravalent

Keggin-POMs had only micropores, which appeared as a sharp peak at 0.59 nm and shoulder at 0.62 nm in the micropore region. The ratios of the external surface areas to the total surface areas of the Cs salts of the tetravalent *Keggin-POMs* were less than 6%. The surface of the Cs salt with *n*-butyl groups showed a hydrophobic nature in comparison with that of the unmodified Cs salt, although the surface density of the *n*-butyl groups was low. On the other hand, the hydroxyl groups present on the surface of the Cs salt barely affected the adsorption properties except for benzene and propanol.

5. Appendix A

Supplementary data associated with this article can be found in the online version, at http://dx.doi.org/10.1016/j.micromeso.xxxxxxxx.

Acknowledgement

This work was supported by KAKENHI (24760634).

References

[1] F. Zamponi, R. Rothhardt, J. Stingl, M. Woerner, T. Elsaesser, PNAS 109 (2012) 7207–5212.

[2] R. Eguchi, S. Uchida, N. Mizuno, J. Phys. Chem. C 116 (2012) 16105–16110.

[3] E.G. Maksimov, V.I. Zinenko, N.G. Zamkova, Physics-USPEKHI 47 (2004) 1075–1099.

[4] T. Saito, T. Tohyama, P.M. Woodward, Y. Shimakawa, Bull. Chem. Soc. Jpn. 84 (2011) 802–806.

[5] H.Z. Cao-Cen, J. Zhao, L.H. Qiu, D. Xu, Q. Li, X.J. Chen, F. Yan, J. Mater. Chem. 22 (2012) 12842–12850.

[6] S. Uchida, R. Eguchi, S. Nakamura, Y. Ogasawara, N. Kurosawa, N. Mizuno, Chem. Mater. 24 (2012) 325–330.

[7] W.Q. Mu, Q.Y. Zhu, L.S. You, X. Zhang, W. Luo, G.Q. Bian, J. Dai, Inorg. Chem. 51 (2012) 1330–1335.

[8] H. Minemawari, J.F.F. Jose, Y. Takahashi, T. Naito, T. Inabe, Bull. Chem. Soc. Jpn. 85 (2012) 335–340.

[9] M. Owczarek, R. Jakubas, V. Kinzhybalo, W. Medycki, D. Kruk, A. Pietraszko, M. Galazka, P. Zielinski, Chem. Phys. Lett. 537 (2012) 38–47.

[10] K. Suzuki, Y. Kikukawa, S. Uchida, H. Tokoro, K. Imoto, S. Ohkoshi, N. Mizuno, Angew.

Chem. Int. Ed. 51 (2012) 1597–1601.

[11] H.-Y An, E.-B. Wang, D.-S. Xiao, Y.-G. Li, Z.-M. Su, L. Xu, Angew. Chem. Int. Ed. 45 (2006) 904–908.

[12] C. Jiang, A. Lesbani, R. Kawamoto, S. Uchida, N. Mizuno, J. Am. Chem. Soc. 128 (2006) 14240–14241.

[13] N. Mizuno, S. Uchida, Chem. Lett. 35 (2006) 688–693.

[14] C. Wang, D. Yang, J. Wang, P. Ma, J. Wang, J. Niu, J. Mol. Struct. 1011 (2012) 1–7.

[15] X. Han, L. Xu, F. Li, N. Jiang, Eur. J. Inorg. Chem. (2011) 4564–4570.

[16] R. Eguchi, S. Uchida, N. Mizuno, Angew. Chem. Int. Ed. 51 (2012) 1635–1639.

[17] S. Uchida, R. Eguchi, N. Mizuno, Angew. Chem. Int. Ed. 49 (2010) 9930–9934.

[18] S. Uchida, N. Mizuno, Coord. Chem. Rev. 252 (2007) 2537–2546.

[19] S. Berndt, D. Herein, F. Zemlin, E. Beckmann, G. Weinberg. J. Schütze, G. Mestl, R. Schlögl, Ber. Bunsenges. Phys. Chem. 102 (1998) 763–774.

[20] K. Inumaru, Catal. Surv. Asia, 10 (2006) 151–160.

[21] G.B. McGarvey, J.B. Moffat, J. Colloid Interface Sci. 125 (1988) 51–60.

[22] J.B. McMonagle, J.B. Moffat, J. Colloid Interface Sci. 101 (1984) 479–488.

[23] J.B. Moffat, J.B. McMonagle, D. Taylor, Solid State Ionics 26 (1988) 191–109.

[24] T. Yamada, K. Johkan, T. Okuhara, Micropore. Mesopore. Mater. 26 (1998) 109–115.

[25] K. Inumaru, H. Nakajima, T. Ito, M. Misono, Chem. Lett. (1996) 559.

[26] T. Okuhara, H. Watanabe, T. Nishimura, K. Inumaru, M. Misono, Chem. Mater. 12 (2000) 2230–2238.

[27] M. Yoshimune, Y. Yoshinaga, T. Okuhara, Micropore. Mesopore. Mater. 51 (2002) 165–174.

[28] Y. Yoshinaga, T. Suzuki, M. Yoshimune, T. Okuhara, Top. Catal. 19 (2002) 179–185.

[29] T. Okuhara, Appl. Catal. A 256 (2003) 213-224.

[30] T. Okuhara, T. Nishimura, M. Misono, in: Proceedings of the 11th International Congress on Catalysis, Stud. Surf. Sci. Catal., vol. 101, 1996, p. 559.

[31] D.B. Taylor, J.B. McMonagle, J.B. Moffat, J. Colloid Interface Sci. 108 (1985) 278–284.

[32] L.R. Pizzio, M.N. Blanco, Micropore. Mesopore. Mater. 103 (2007) 40–47.

[33] T.X. Bui, S.-Y. Kang, S.-H. Lee, H. Choi, J. Hazard. Mater. 193 (2011) 156–163.

[34] J. Bu, H.-K, Rhee, Catal. Lett. 65 (2000) 141–145.

[35] M.C. Capel-Sanchez, L. Barrio, J.M. Campos-Martin, J.L.G. Fierro, J. Colloid Interface Sci. 277 (2004) 146–153.

[36] L. Liu, R. Singh, G. Li, G. Xiao, P.A. Webley, Y. Zhai, Mater. Chem. Phys. 133 (2012) 1144–1151.

[37] Y. Kuwahara, T. Kamegawa, K. Mori, H. Yamashita, Chem. Commun. (2008) 4783–4785.

[38] K. Inumaru, Y. Inoue, S. Kakii, T. Nakano, S. Yamanaka, Phys. Chem. Chem. Phys. 6 (2004) 3133–3139.

[39] Y. Kamiya, S. Sano, Y. Miura, Y. Uchida, Y. Ogawa, Y. Iwase, T. Okuhara, Chem. Lett. 39 (2010) 881–883.

[40] B. Matt. J. Moussa, L.-M. Chamoreau, C. Afonso, A. Proust, H. Amouri, G. Izzet, Organometallics 31 (2012) 35–38.

[41] G.S. Chorghade, M.T. Pope, J. Am. Chem. Soc. 109 (1987) 5134–5138.

[42] T. Okuhara, N. Mizuno, M. Misono, Adv. Catal. 41 (1996) 113–252.

[43] N. Mizuno, M. Misono, Chem. Lett. (1987) 967–970.

[44] M.S. Kaba, I.K Song, D.C. Duncan, C.L. Hill, M.A. Barteau, Inorg. Chem. 37 (1998) 398–406.

[45] T. Yamada, T. Okuhara, Langmuir 16 (2000) 2321–2325.

[46] K. Inumaru, S. Kakii, H. Yoshida, S. Yamanaka, Chem. Lett. 39 (2010) 1215–1217.

[47] G.R. Desiraju, Acc. Chem. Res. 35 (2002) 565–573.

[48] M. Nishio, Tetrahedron 61 (2005) 6923–6950.

Table 1

Elemental analysis of the Cs salts.

Sample	Elemental analysis/wt%[a)]								Formula[b)]
	P	Si	W	Sn	Cs	K	C	H	
Cs_3-PW12	0.92	---	65.1	---	11.6	0.0	---	---	$Cs_3[PW_{12}O_{40}]\cdot 6H_2O$
	(0.92)		(65.2)		(11.8)	(0.0)			
Cs_4-SiW12	---	0.86	61.6	---	14.8	0.0	---	---	$Cs_4[SiW_{12}O_{40}]\cdot 9H_2O$
		(0.80)	(61.8)		(14.9)	(0.0)			
Cs_4-PW11(Sn-*n*-Bu)	0.79	---	57.6	3.06	14.8	---	1.40	0.68	$Cs_4[PW_{11}O_{39(}Sn\text{-}n\text{-}C_4H_9)]\cdot 8H_2O$
	(0.88)		(57.3)	(3.36)	(15.1)		(1.36)	(0.71)	
Cs_4-PW11(Sn-OH)	0.91	---	58.6	3.57	13.9	0.45	---	---	$Cs_{3.6}K_{0.4}[PW_{11}O_{39(}Sn\text{-}OH)]\cdot 8H_2O$
	(0.90)		(58.6)	(3.44)	(13.9)	(0.45)			

a) Figures in parenthesis are the values calculated from the formulae.

b) Number of crystalline water was estimated from the weight loss in TG profile.

Table 2

Lattice constants, crystallite sizes, surface areas, and micropore volumes for the Cs salts.

Negative charge of heteropoly anion	Sample	Lattice constant /nm	Crystallite size /nm	Surface area[a)]/m^2 g^{-1}		Micropore volume[b)] /cm^3 g^{-1}	S_{os}[c)] /m^2 g^{-1}	V_{defect}[d)] /cm^3 g^{-1}
				Total	External surface			
–3	**Cs_3-PW12**	1.182	11.7	136	100	----	89	----
–4	**Cs_4-SiW12**	1.178	45.3	168	8	0.056	20	0.041
	Cs_4-PW11(Sn-*n*-Bu)	1.179	50.9	208	3	0.074	18	0.042
	Cs_4-PW11(Sn-OH)	1.180	34.0	177	10	0.055	27	0.042

a) Surface area was estimated from the slopes of the *t*-plots calculated from N_2 adsorption isotherms.

b) Micropore volume was estimated from the intercept of line B in the *t*-plot shown in Fig. 6.

c) Surface area of the outer surface of crystallite calculated from crystallite size (XRD) and real density by using eq. 3.

d) Total volume of the anion vacancies per unit weight of the Cs salt calculated by using eqs. 4 and 5.

Figure captions

Fig. 1 Polyhedral representations of tetravalent Keggin-type polyoxometalates. (a) $[SiW_{12}O_{40}]^{4-}$, (b) $[PW_{11}O_{39}(Sn\text{-}n\text{-}C_4H_9)]^{4-}$, and (c) $[PW_{11}O_{39}(Sn\text{-}OH)]^{4-}$. ( ) Sn,) O,) C, and ( ) H.

Fig. 2. (A) ^{31}P NMR spectra of (a) $[PW_{12}O_{40}]^{3-}$, (b) $[PW_{11}O_{39}]^{7-}$, (c) $[PW_{11}O_{39}(Sn\text{-}n\text{-}C_4H_9)]^{4-}$, and (d) $[PW_{11}O_{39}(Sn\text{-}OH)]^{4-}$ in 5:1 H_2O/D_2O (v/v) and (B) solid-state ^{31}P MAS NMR spectra of (e) **Cs_3-PW12**, (f) **Cs_4-PW11(Sn-*n*-Bu)**, and (g) **Cs_4-PW11(Sn-OH)**.

Fig. 3. IR spectra of (a) **Cs_3-PW12**, (b) **K_7-PW11**, (c) **Cs_4-PW11(Sn-*n*-Bu)**, (d) **Cs_4-PW11(Sn-OH)**, and (e) **Cs_4-SiW12**. All the samples were diluted with KBr to 0.5 wt%.

Fig. 4. TG-DTA profiles in air for (a) **Cs_3-PW12**, (b) **Cs_4-PW11(Sn-*n*-Bu)**, (c) **Cs_4-PW11(Sn-OH)**, and (d) **Cs_4-SiW12**.

Fig. 5. XRD patterns for (a) **Cs_3-PW12**, (b) **Cs_4-SiW12,** (c) **Cs_4-PW11(Sn-*n*-Bu)**, and (d) **Cs_4-PW11(Sn-OH)**.

Fig. 6. Adsorption-desorption isotherms of N_2 at 77 K for (a) **Cs_3-PW12**, (b) **Cs_4-SiW12,** (c) **Cs_4-PW11(Sn-*n*-Bu)**, and (d) **Cs_4-PW11(Sn-OH)**. Insets are *t*-plots calculated from corresponding N_2 adsorption isotherms.

Fig. 7. Micropore and mesopore size distributions for (a) **Cs_3-PW12**, (b) **Cs_4-SiW12,** (c) **Cs_4-PW11(Sn-*n*-Bu)**, and (d) **Cs_4-PW11(Sn-OH)**.

Fig. 8. Model of crystalline structure of (A) a Cs salt of a trivalent *Keggin-POM*, like **Cs_3-PW12**, and (B) a Cs salt of a tetravalent *Keggin-POM*, like **Cs_4-SiW12, Cs_4-PW11(Sn-*n*-Bu)**, and **Cs_4-PW11(Sn-OH)**. Only heteropoly anions are depicted in the illustrations, although there are cesium ions located between two heteropoly anions. The unit cells expand in the vertical direction. In structure B, a quarter of the heteropoly anions have defects to avoid the mismatch in the Cs^+/(heteropoly anion) ratios required for charge balance (= 4) and for a bcc structure (= 3), and these anion defects form micropores.

Fig. 9. Adsorption isotherms of water, methanol, ethanol, 1-propanol, benzene, and *n*-hexane on microporous Cs salts. (○) **Cs_4-SiW12,** (▲) **Cs_4-PW11(Sn-*n*-Bu)**, and (■) **Cs_4-PW11(Sn-OH)**.

Fig. 10. Schematic images of (A) an *n*-butyl group on the surface of **Cs_4-PW11(Sn-*n*-Bu)** and (B) a hydroxyl group on the surface of **Cs_4-PW11(Sn-OH)**.

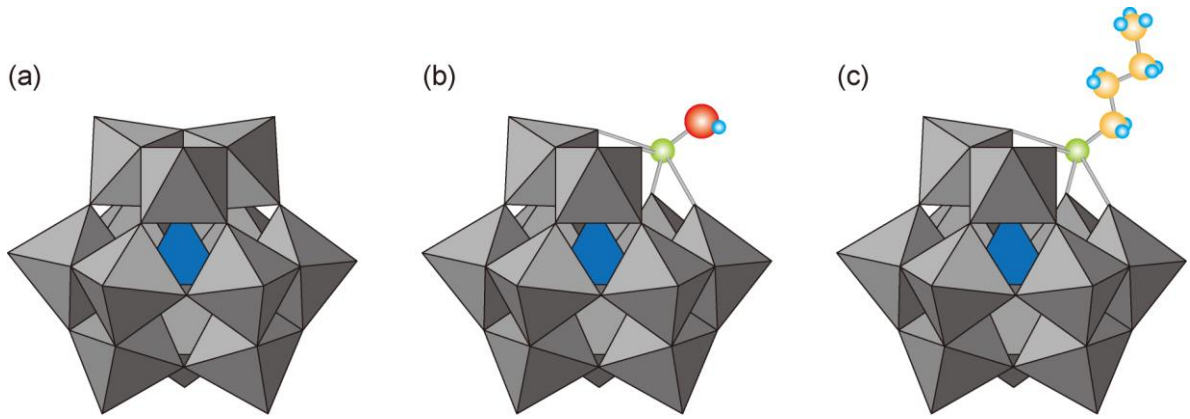

Fig. 1 Polyhedral representations of tetravalent Keggin-type polyoxometalates. (a) $[SiW_{12}O_{40}]^{4-}$, (b) $[PW_{11}O_{39}(Sn\text{-}n\text{-}C_4H_9)]^{4-}$, and (c) $[PW_{11}O_{39}(Sn\text{-}OH)]^{4-}$. ( ) Sn, ( ) O, ( ) C, and ( ) H.

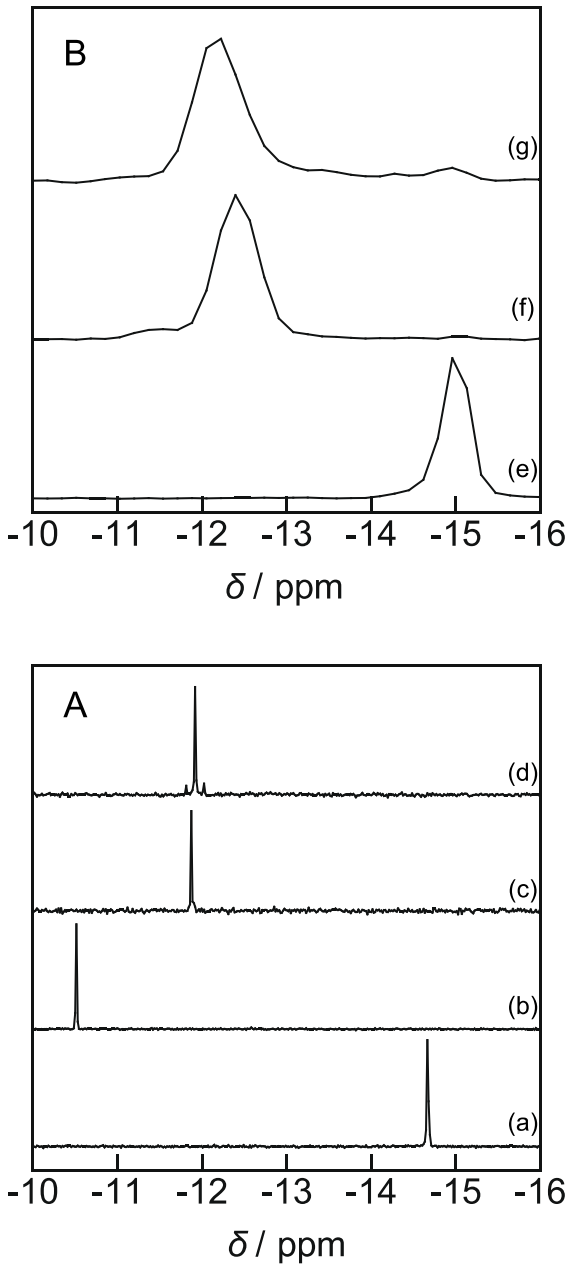

Fig. 2. (A) ^{31}P NMR spectra of (a) $[PW_{12}O_{40}]^{3-}$, (b) $[PW_{11}O_{39}]^{7-}$, (c) $[PW_{11}O_{39}(Sn\text{-}n\text{-}C_4H_9)]^{4-}$, and (d) $[PW_{11}O_{39}(Sn\text{-}OH)]^{4-}$ in 5:1 H_2O/D_2O (v/v) and (B) solid-state ^{31}P MAS NMR spectra of (e) **Cs_3-PW12**, (f) **Cs_4-PW11(Sn-*n*-Bu)**, and (g) **Cs_4-PW11(Sn-OH)**.

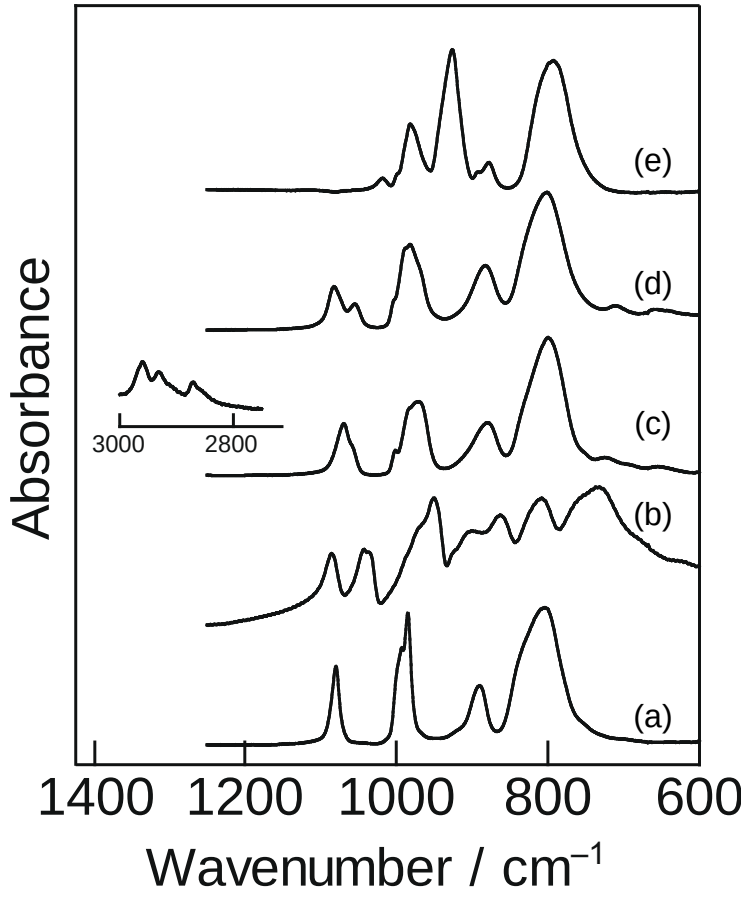

Fig. 3. IR spectra of (a) **Cs_3-PW12**, (b) **K_7-PW11**, (c) **Cs_4-PW11(Sn-*n*-Bu)**, (d) **Cs_4-PW11(Sn-OH)**, and (e) **Cs_4-SiW12**. All the samples were diluted with KBr to 0.5 wt%.

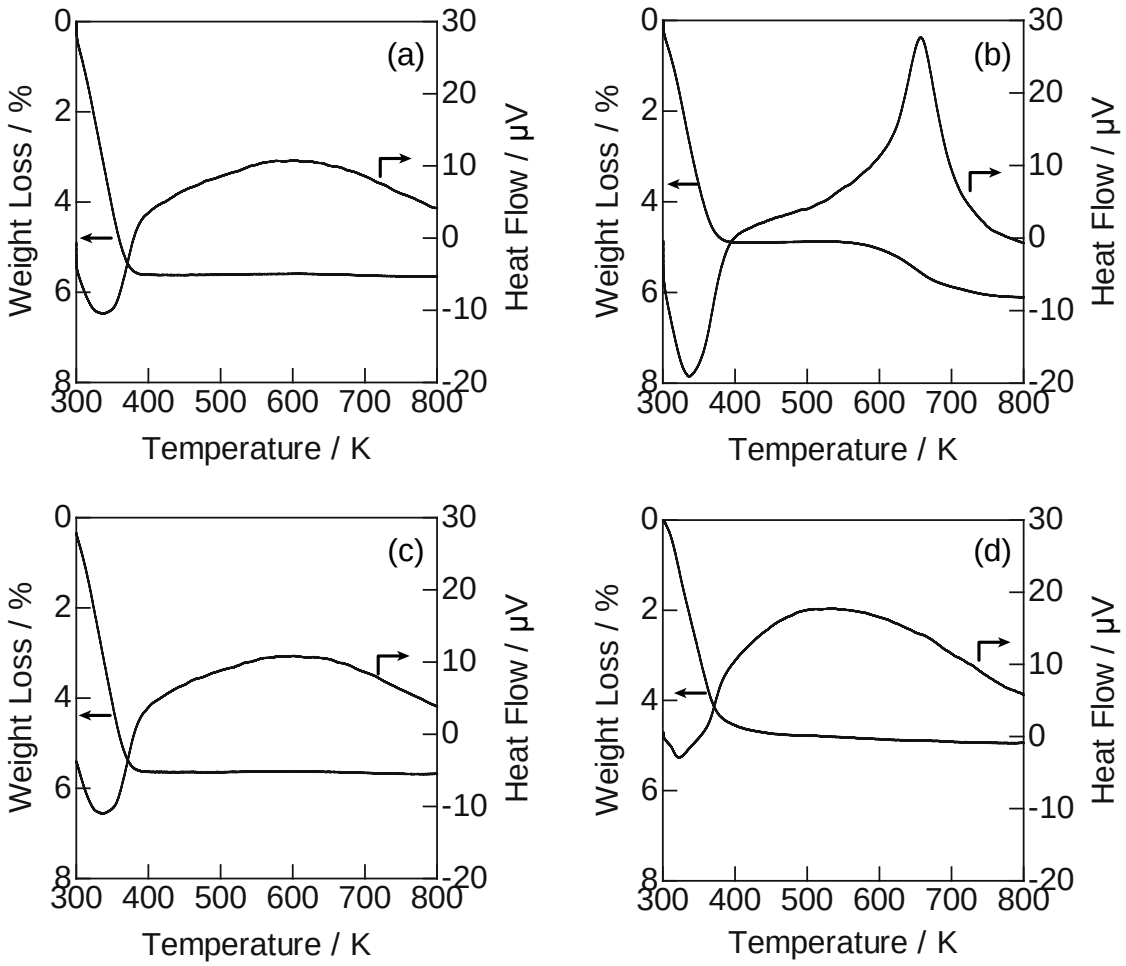

Fig. 4. TG-DTA profiles in air for (a) **Cs_3-PW12**, (b) **Cs_4-PW11(Sn-*n*-Bu)**, (c) **Cs_4-PW11(Sn-OH)**, and (d) **Cs_4-SiW12**.

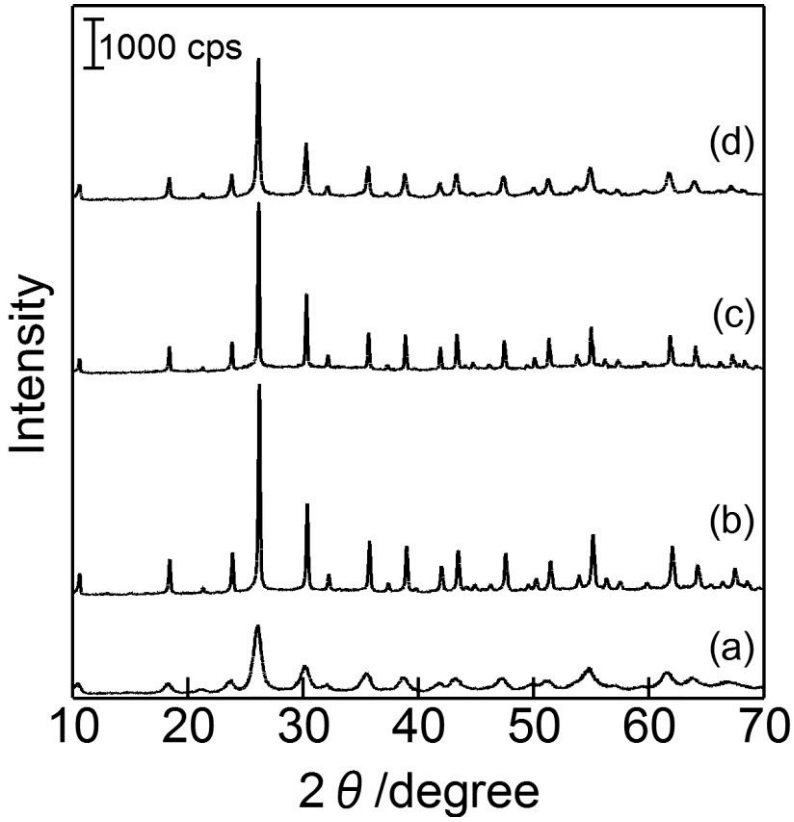

Fig. 5. XRD patterns for (a) **Cs_3-PW12**, (b) **Cs_4-SiW12,** (c) **Cs_4-PW11(Sn-*n*-Bu)**, and (d) **Cs_4-PW11(Sn-OH)**.

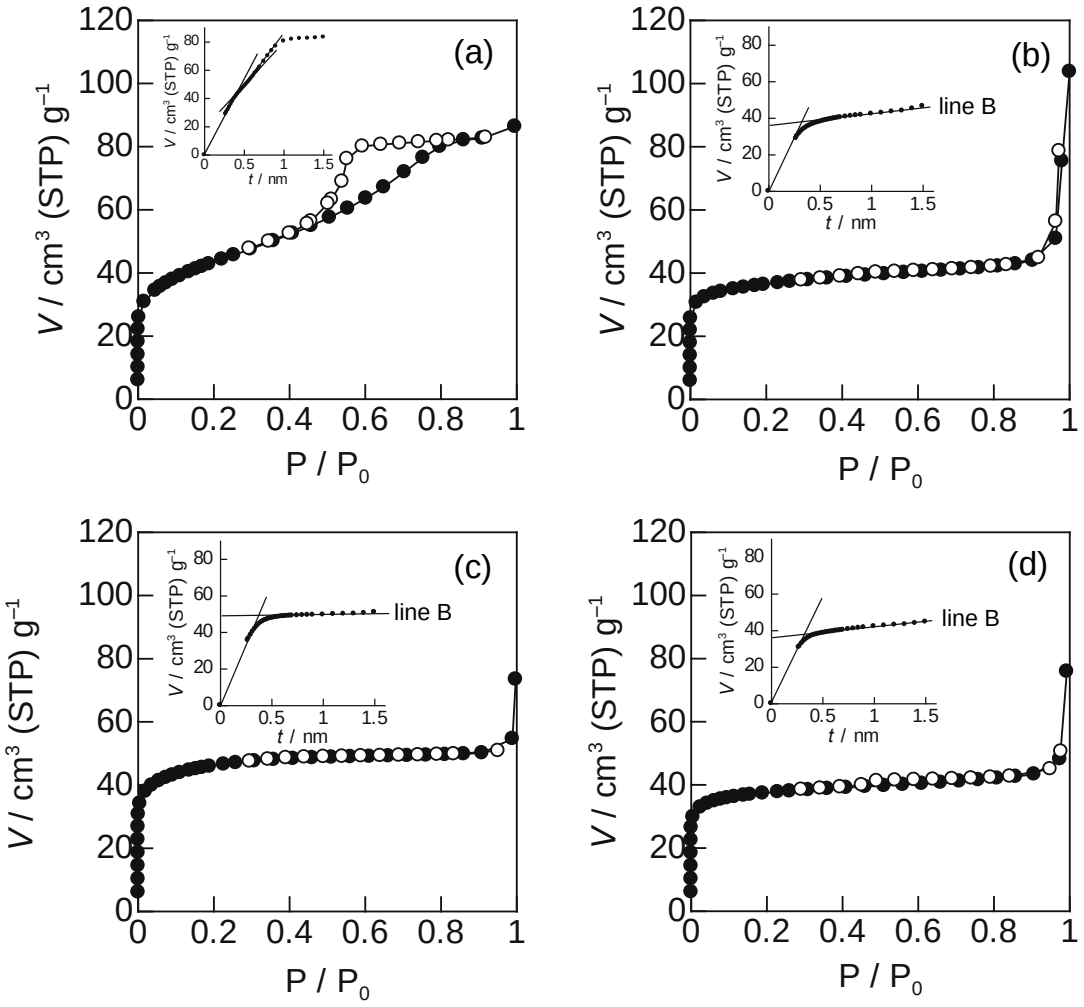

Fig. 6. Adsorption-desorption isotherms of N_2 at 77 K for (a) **Cs_3-PW12**, (b) **Cs_4-SiW12,** (c) **Cs_4-PW11(Sn-*n*-Bu)**, and (d) **Cs_4-PW11(Sn-OH)**. Insets are *t*-plots calculated from corresponding N_2 adsorption isotherms.

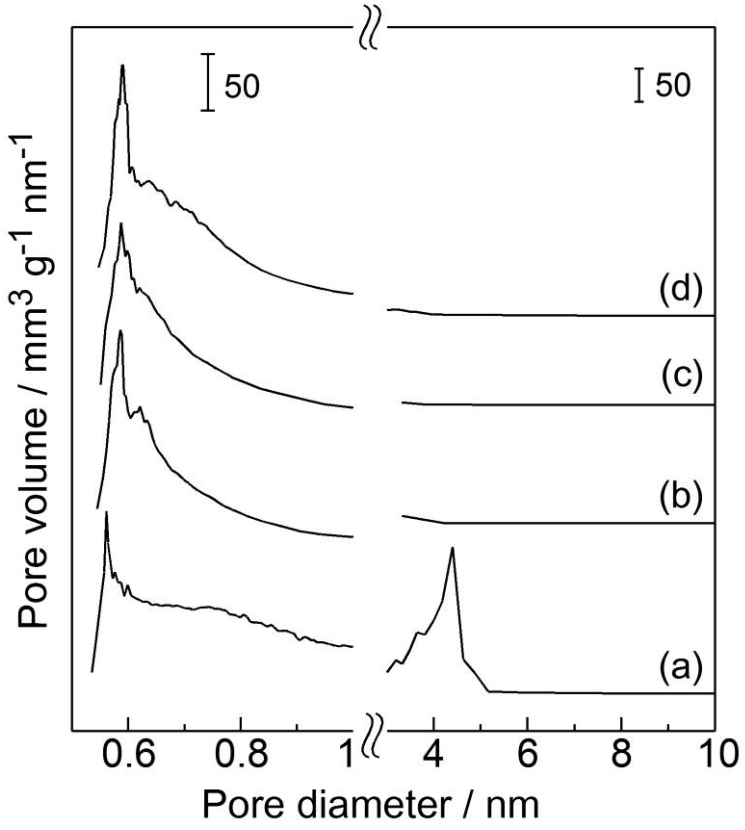

Fig. 7. Micropore and mesopore size distributions for (a) **Cs_3-PW12**, (b) **Cs_4-SiW12,** (c) **Cs_4-PW11(Sn-*n*-Bu)**, and (d) **Cs_4-PW11(Sn-OH)**.

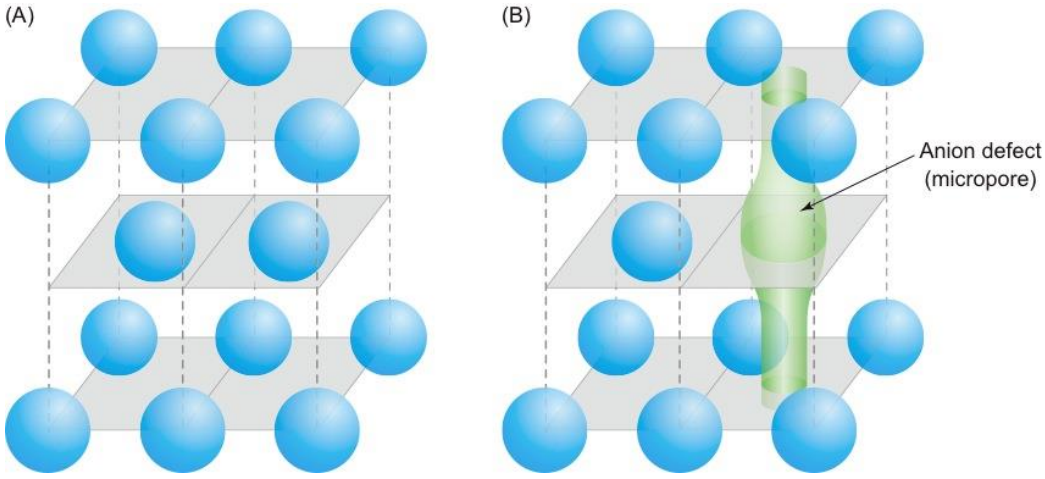

Fig. 8. Model of crystalline structure of (A) a Cs salt of a trivalent *Keggin-POM*, like **Cs_3-PW12**, and (B) a Cs salt of a tetravalent *Keggin-POM*, like **Cs_4-SiW12, Cs_4-PW11(Sn-*n*-Bu)**, and **Cs_4-PW11(Sn-OH)**. Only heteropoly anions are depicted in the illustrations, although there are cesium ions located between two heteropoly anions. The unit cells expand in the vertical direction. In structure B, a quarter of the heteropoly anions have defects to avoid the mismatch in the Cs^+/(heteropoly anion) ratios required for charge balance (= 4) and for a bcc structure (= 3), and these anion defects form micropores.

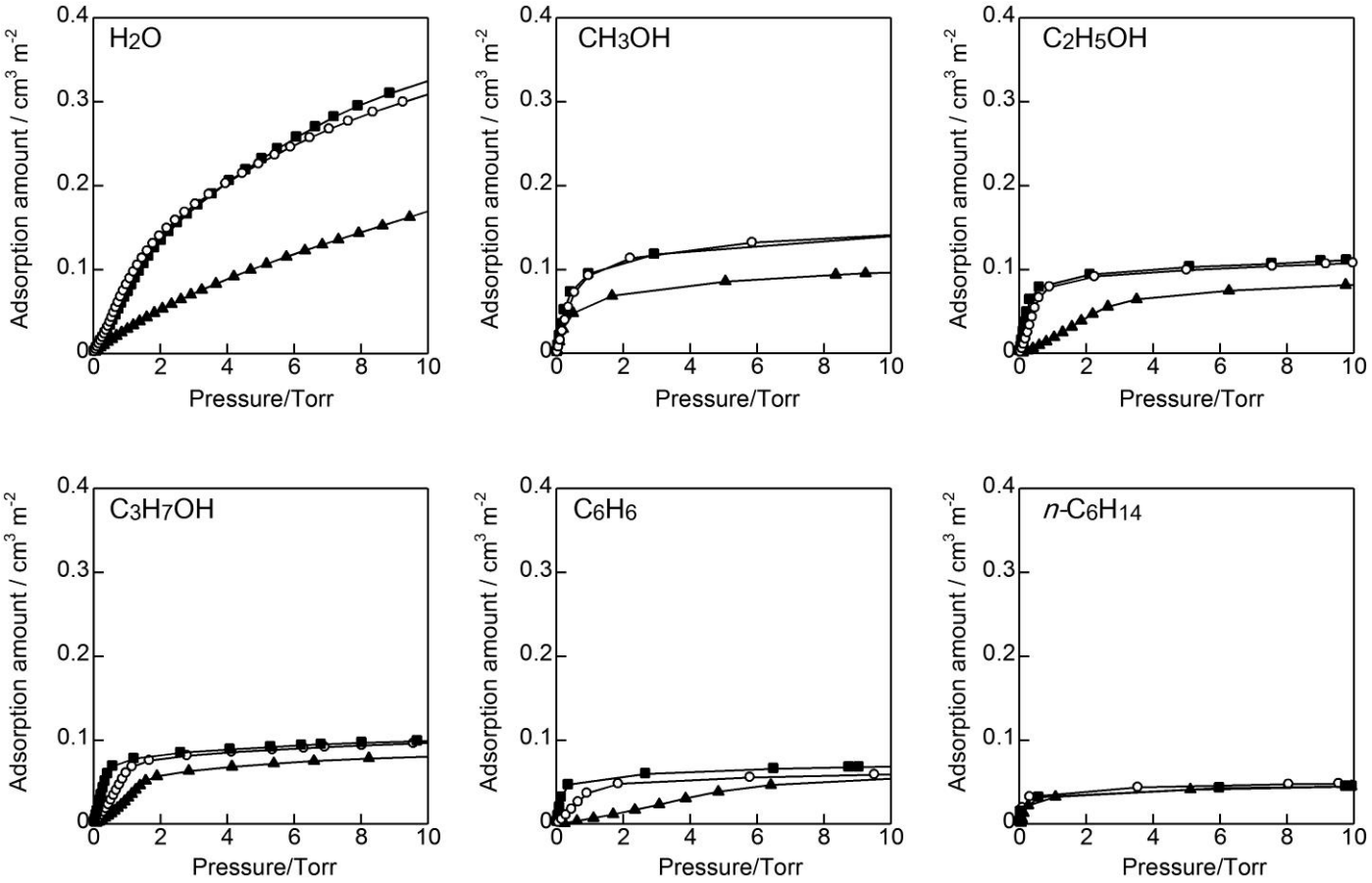

Fig. 9. Adsorption isotherms of water, methanol, ethanol, 1-propanol, benzene, and *n*-hexane on microporous Cs salts. (○) **Cs_4-SiW12,** (▲) **Cs_4-PW11(Sn-*n*-Bu)**, and (■) **Cs_4-PW11(Sn-OH)**.

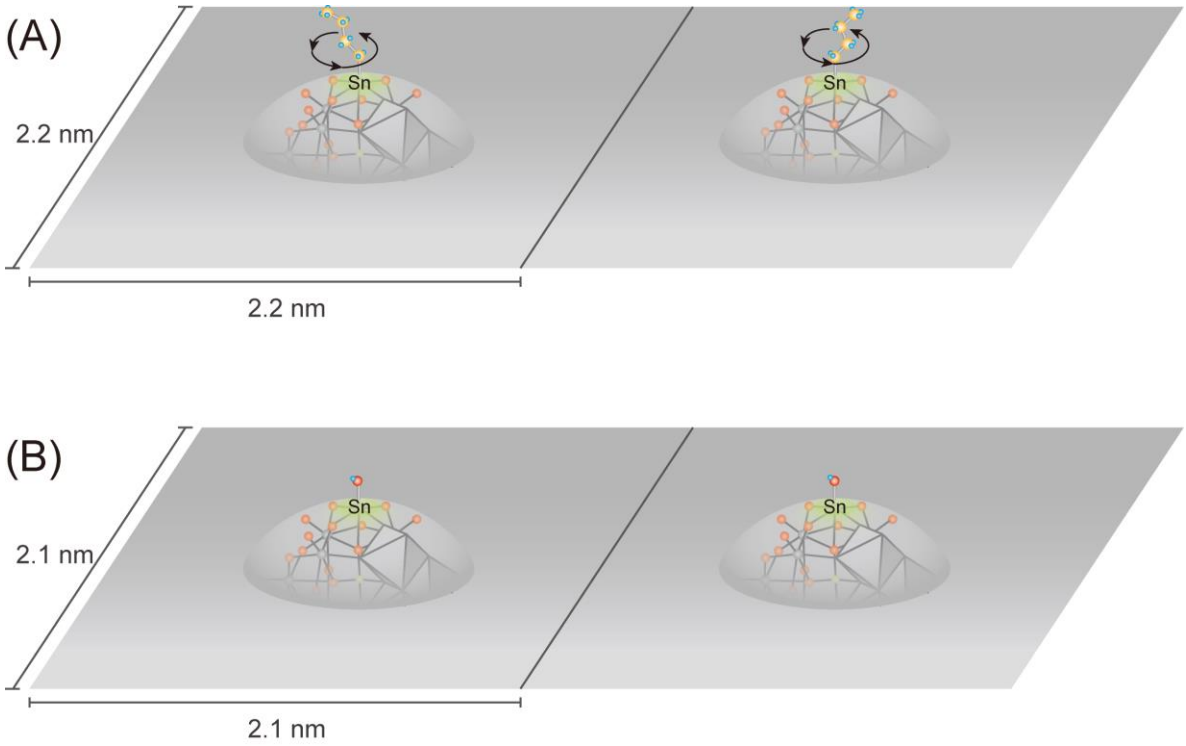

Fig. 10. Schematic images of (A) an *n*-butyl group on the surface of **Cs_4-PW11(Sn-*n*-Bu)** and (B) a hydroxyl group on the surface of **Cs_4-PW11(Sn-OH)**.